

NON-AXISYMMETRIC ABERRATION PATTERNS FROM WIDE-FIELD TELESCOPES USING SPIN-WEIGHTED ZERNIKE POLYNOMIALS

STEPHEN M. KENT¹

¹*Fermi National Accelerator Laboratory
MS/127
P.O. Box 500
Batavia, IL 60510, USA*

ABSTRACT

If the optical system of a telescope is perturbed from rotational symmetry, the Zernike wavefront aberration coefficients describing that system can be expressed as a function of position in the focal plane using spin-weighted Zernike polynomials. Methodologies are presented to derive these polynomials to arbitrary order. This methodology is applied to aberration patterns produced by a misaligned Ritchey-Chrétien telescope and to distortion patterns at the focal plane of the DESI optical corrector, where it is shown to provide a more efficient description of distortion than conventional expansions.

Keywords: methods: analytical - telescopes

1. INTRODUCTION

Uncorrected aberrations in telescope optics often affect one’s ability to extract science from images at the telescope focal plane. For example, in weak lensing science, where one measures distortions in the images of galaxies induced by gravitational lensing from foreground mass concentrations, one’s measurements are particularly affected by low-order aberrations such as coma and astigmatism, which induce ellipticities in images that mimic the effects of gravitational lensing (eg., [Jarvis et al. 2008](#); [Jee & Tyson 2011](#); [Hamana 2013](#)). Furthermore, the operation of certain instruments, such as fiber positioners systems used for multiobject spectroscopy, require detailed knowledge of the focal plane distortion pattern ([Akiyama 2008](#); [Kent et al. 2016](#)). It is often desirable to have an analytic model to parametrize the aberration pattern across the focal plane. For an axisymmetric system, the aberrations depend only on radial distance from the symmetry axis, and thus the patterns can be characterized with 1–d radial polynomials. However, even for well-aligned telescopes, the patterns will generally have non-axisymmetric components, so a more general formulation is desired. This paper presents such a formulation based on the use of spin-weighted functions.

2. THEORY

Figure 1 shows the geometry of the exit pupil and focal plane. The wavefront errors that give rise to optical aberrations can be characterized in terms of Zernike polynomials, which decompose the wavefront shape into orthogonal functions of the exit pupil polar coordinates (ρ, ψ) . At a particular point in the focal plane, one can write:

$$W(\rho, \psi) = \sum_l \sum_s [A_{ls} \cos s\psi + B_{ls} \sin s\psi] R_l^s(\rho), \quad (1)$$

where W is the wavefront error (in units, say, of microns or waves), $R_l^s(\rho)$ is a Zernike radial polynomial, and A_{ls}, B_{ls} are Zernike aberration coefficients (see, e.g., [Born & Wolf 2000](#)). Indices l and s are restricted to combinations where $l + s$ is even and $s \leq l$. (For reasons that will be apparent below, l and s are used here for pupil polynomial indices, while the more conventional n and m indices are reserved for the focal plane.)

The Zernike aberration coefficients A, B are themselves a function of polar coordinates (r, ϕ) in the focal plane, so in general one can write them as $A_{ls}(r, \phi)$ and $B_{ls}(r, \phi)$. The goal of this paper is to develop efficient polynomial expressions for these coefficients.

The orientation of the pupil coordinate system with respect to the focal plane coordinates needs to be specified. Normally, the pupil plane x and y axes are aligned with those of the focal plane, forming a global Cartesian system. However, for an axisymmetric system, a more natural pupil coordinate system is one in which the angle ψ is replaced with $\psi' = \psi - \phi$ at each location in the focal plane such that the axes of the pupil system are always oriented in the radial and tangential directions relative to the optical axis (e.g., [Braat & Janssen 2013](#)). In this case, the aberration coefficients depend only on radial distance from the symmetry axis, and the patterns can be characterized with 1–d radial polynomials. If the system is perturbed from a state of axisymmetry, e.g., as happens when

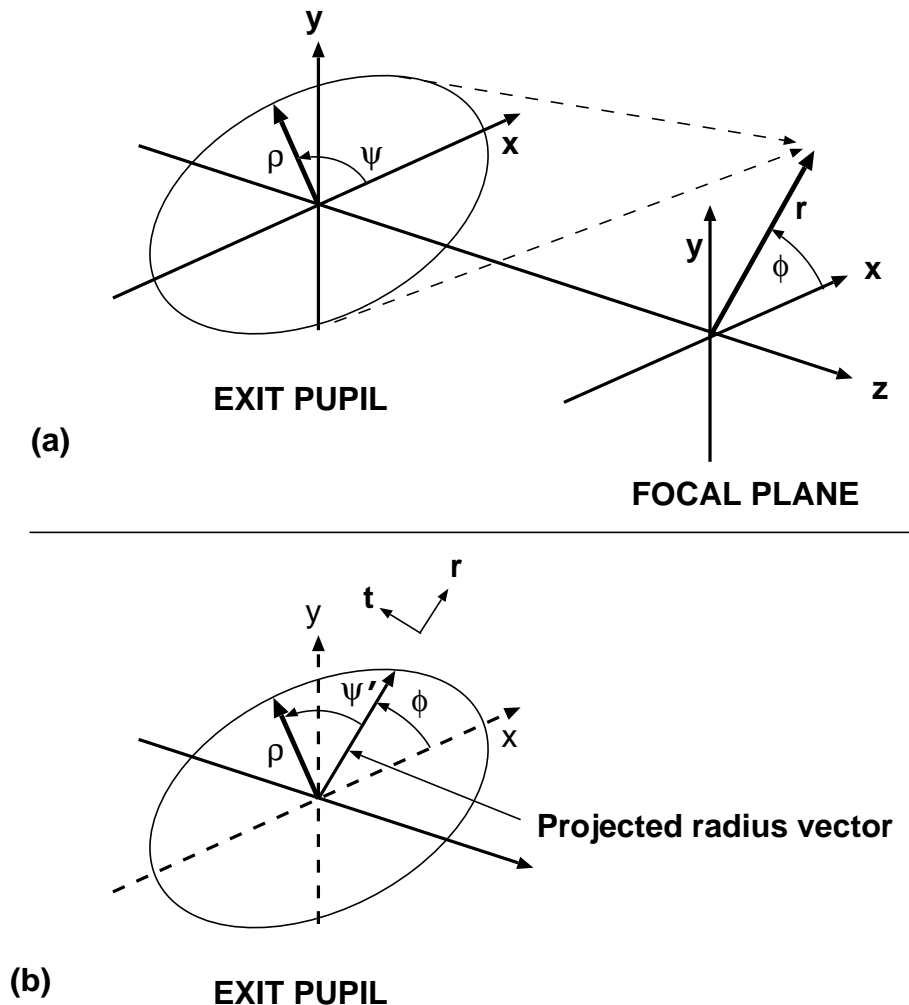


Figure 1. (a) Schematic diagram showing the orientation and coordinate system definitions of the pupil plane (ρ, ψ) and focal plane (r, ϕ). Each point in the focal plane (e.g., at radius vector \vec{r}) sees an image of the exit pupil. A global Cartesian (x, y) system is illustrated. (b) Another diagram of the pupil plane, this time showing the projection of the radius vector \mathbf{r} onto the pupil plane. One can define local pupil axes (r, t) that are aligned parallel and perpendicular to the projected radius vector and that are rotated by ϕ relative to the global (x, y) axes. Pupil coordinates in this system are given by ρ and $\psi' = \psi - \phi$.

the optical elements are misaligned or the corrector contains a non-axisymmetric element such as an atmospheric dispersion compensator (ADC), this axisymmetric formulation is no longer applicable. However, the system still retains a high degree of symmetry, and thus it seems desirable to seek a more general formulation for the aberration pattern that still retains the radial/tangential property such that it reduces to the axisymmetric form in the limit of zero perturbation.

Figure 2 illustrates the situation. This figure shows the astigmatism pattern at the focal plane of a typical two-mirror telescope. (The telescope is defocused slightly to highlight the orientation of the pattern.) In Fig. 2(a), the telescope is properly aligned, and the pattern is axisymmetric. In Fig. 2(b), the secondary mirror is offset, then tilted to remove first-order coma; the astigmatism pattern is now perturbed, but it still retains a high degree of

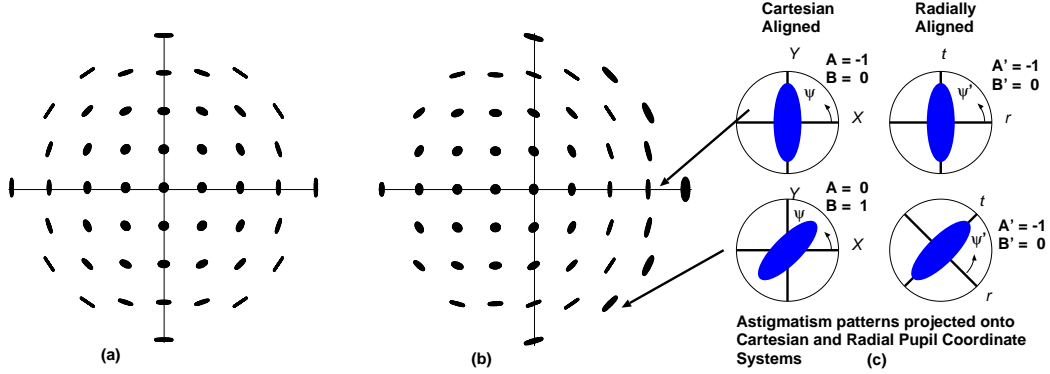


Figure 2. Astigmatism patterns as a function of location in the focal plane for (a) aligned 2-mirror telescope and (b) misaligned telescope with secondary mirror displaced and tilted. Right panel (c) shows the projection of astigmatism pattern onto Cartesian (A, B) and radially aligned (A', B') pupil axes. The senses of the pupil azimuth angles ψ and ψ' are also shown. The units are arbitrary.

symmetry. In Fig. 2(c), the values for the aberration coefficients at two locations in the focal plane are shown schematically when expressed using both a Cartesian-aligned pupil coordinate system (left; A and B) and a radially-aligned system (right; A' and B'). In the former, the astigmatism amplitude oscillates between the A and B terms as one moves about the focal plane, even if the total amplitude is constant. In the latter, the amplitude is almost entirely in the A' (radial) component, thus providing a clearer measure of the perturbation pattern.

Multiple formulations for the dependence of aberration coefficients on focal plane coordinates have appeared in the literature over the years, primarily in connection with the problem of aligning telescopes with wide-field focal planes, (e.g., Shack & Thompson 1980; McLeod 1996; Schechter & Levinson 2011). One approach is to express the aberration coefficients themselves as a function of focal plane coordinates using the same Zernike polynomial basis (e.g., Kwee & Braat 1993). Although such an expansion is straightforward to construct, the aberration coefficients are still referenced to pupil axes that are aligned with a global Cartesian system across the focal plane.

One can easily apply a rotation to the equations for the aberration coefficients when expressed in a Cartesian-aligned pupil system in order to convert them to a radially-aligned system, but the resulting expansions are no longer of Zernike form. Various alternative expansions using Zernike polynomials or products of Zernike polynomials have also been proposed (e.g., Agurok 1998; Manuel 2009) but these are still not quite of the desired form. Gray & Rolland (2015) came the closest, developing expansions in the desired form up to eighth order in radius and third order in azimuth by using methods of Geometric Algebra, but the resulting expressions are not easily generalized to arbitrary order.

This difficulty suggests approaching the problem from a different direction. From Eq. (1), one can show that, for a particular l, s combination, the quantity $A_{ls} + iB_{ls}$, expressed as a function of (r, ϕ) , is a field of spin-weight s . Such a field can be derived from a scalar field by successive application of spin raising operators (a process analogous to the

use of angular momentum raising operators in quantum mechanics.) This approach turns out to be fruitful.

Spin-weighted functions are not commonly used in optics, so a short review is presented here. (See also Newman & Penrose 1966; Goldberg et al. 1967; Torres del Castillo 1992). Consider a local Cartesian system (x, y) centered on some particular location in the focal plane with basis vectors $\mathbf{e}_1, \mathbf{e}_2$ forming a right-handed system. A function ${}_sF(x, y)$ is said to have spin-weight s if, under a counterclockwise rotation of $\mathbf{e}_1, \mathbf{e}_2$ by angle ϕ (i.e., $\mathbf{e}_1' + i\mathbf{e}_2' = e^{-i\phi}[\mathbf{e}_1 + i\mathbf{e}_2]$), the field in the rotated coordinate frame transforms as ${}_sF' = e^{-is\phi} {}_sF$. (The sign convention is chosen to match that of the CMB polarization literature.) Thus, if one rewrites the coefficients of each term in Eq. (1) in the form

$$A \cos s\psi + B \sin s\psi = \frac{1}{2}(A - iB)e^{is\psi} + \frac{1}{2}(A + iB)e^{-is\psi}, \quad (2)$$

the coefficients of the terms on the right side have spin-weights $-s$ and $+s$ respectively.

As an example, consider an optical system for which the wavefront error includes terms corresponding to astigmatism. At a particular point in the focal plane (x, y) , the two relevant terms for the wavefront error are $A_{22}\rho^2 \cos 2\psi$ and $B_{22}\rho^2 \sin 2\psi$ (Z6 and Z5 in the nomenclature of Noll 1976). The complex quantity formed from the two coefficients, ${}_2F = A_{22} + iB_{22}$, expressed as a function of focal plane coordinates (x, y) , has spin-weight $s = +2$. To demonstrate this property, let (x', y') be another pupil coordinate system centered at this point and rotated counterclockwise with respect to the (x, y) system by an angle ϕ . In the new coordinate system, the complex coefficient should be given by ${}_2F' = A'_{22} + iB'_{22} = {}_2F e^{-2i\phi}$. Equating the real and imaginary parts, the coefficients transform as:

$$A'_{22} = A_{22} \cos 2\phi + B_{22} \sin 2\phi, \quad (3a)$$

$$B'_{22} = B_{22} \cos 2\phi - A_{22} \sin 2\phi \quad (3b)$$

or

$$A_{22} = A'_{22} \cos 2\phi - B'_{22} \sin 2\phi, \quad (4a)$$

$$B_{22} = B'_{22} \cos 2\phi + A'_{22} \sin 2\phi. \quad (4b)$$

The wavefront error itself at that point is given by:

$$W = A_{22}\rho^2 \cos 2\psi + B_{22}\rho^2 \sin 2\psi \quad (5a)$$

$$= A'_{22}\rho^2 \cos 2(\psi - \phi) + B'_{22}\rho^2 \sin 2(\psi - \phi) \quad (5b)$$

$$= A'_{22}\rho^2 \cos 2\psi' + B'_{22}\rho^2 \sin 2\psi', \quad (5c)$$

where $\psi' = \psi - \phi$. Thus, the form of the wavefront aberration is the same in the rotated frame as it is in the original frame. If one rotates by 180° degrees, the coefficients themselves in the new frame are unchanged from the old frame. More generally, for any field of spin-weight s , a local rotation of $360^\circ/s$ leaves the coefficients unchanged.

A key property of spin-weighted fields is that a field of positive spin-weight s can be generated from a scalar/pseudo-scalar field ${}_0F = S - iK$ (with functions S and K being real) by s applications of the spin raising operator. In Cartesian coordinates, each step is of the form:

$${}_{s+1}F = \eth {}_sF = - \left[\frac{\partial}{\partial x} + i \frac{\partial}{\partial y} \right] {}_sF. \quad (6)$$

(The symbol “ \eth ” was first used for this purpose by [Newman & Penrose 1966](#)). This result can be verified by examining the rotational properties of ${}_{s+1}F$. The real and imaginary parts correspond to curl-free and divergence-free fields respectively, and, by analogy to electromagnetism, this formulation is sometimes referred to as E/B mode decomposition, a terminology that will be used here as well. For negative s , one takes the complex conjugate of Eq. (6) to create a spin lowering function $\bar{\eth}$. For simplicity, only $s \geq 0$ will be considered in what follows, since the equations for negative s contain no additional information.

Such an approach is commonly used in problems involving spin-weight 1 fields, such as atmospheric distortion ([Bernstein et al. 2017](#)), and spin-weight 2 fields, such as gravitational radiation ([Newman & Penrose 1966](#)), weak lensing ([Stebbins 1996](#)), and Cosmic Microwave Background polarization ([Kamionkowski et al. 1997](#); [Zaldarriaga & Seljak 1997](#)). For the spin-weight 2 problems, one normally uses spherical coordinates and expands the potentials using spherical harmonics. Here, the natural coordinates are polar (r, ϕ) , and the preferred choice for the radial functions is, again, Zernike radial polynomials (although other choices – e.g. Bessel function – are possible; [Trevino et al. 2013](#)). One can transform from Cartesian to polar coordinates as follows. Let:

$${}_sF' = e^{-is\phi} {}_sF, \quad (7a)$$

$${}_{s+1}F' = e^{-i(s+1)\phi} {}_{s+1}F, \quad (7b)$$

$$\left[\frac{\partial}{\partial x} + i \frac{\partial}{\partial y} \right] {}_sF = e^{i\phi} \left[\frac{\partial}{\partial r} + \frac{i}{r} \frac{\partial}{\partial \phi} \right] {}_sF. \quad (7c)$$

Upon substituting these expressions into Eq. (6), one finds that the raising and lowering operators in polar coordinates are given by ([Torres del Castillo 1992](#)):

$$\eth {}_sF = - \left[\frac{\partial}{\partial r} - \frac{s}{r} + \frac{i}{r} \frac{\partial}{\partial \phi} \right] {}_sF, \quad (8a)$$

$$\bar{\eth} {}_sF = - \left[\frac{\partial}{\partial r} + \frac{s}{r} - \frac{i}{r} \frac{\partial}{\partial \phi} \right] {}_sF. \quad (8b)$$

Common Zernike wavefront terms in Eq. (1) can be classified as spin-weight 0 (defocus; spherical aberration), spin-weight 1 (distortion, coma), spin-weight 2 (astigmatism), spin-weight 3 (trefoil), and spin-weight 4 (quadrafoil). Generically, the coefficients for each type of aberration are given by:

$$A'_{ls} + iB'_{ls} = {}_sF' = \eth^s (S_{ls} - iK_{ls}), \quad (9)$$

where the notation δ^s means s applications of the spin-raising operator (going from spin-weight 0 to spin-weight s) and the prime ($'$) again indicates that the pupil coordinate system (ρ, ψ') , where $\psi' = \psi - \phi$ is rotated to align the axes in the radial and tangential directions at any location in the focal plane. Each aberration type (e.g., third-order coma) corresponds to a particular pair of (l, s) values (e.g., $l = 3, s = 1$) for which there is a corresponding pair of scalar potentials S_{ls}, K_{ls} . Given these potentials, the aberration coefficients are derived as follows:

Spin-weight 0:

$$A'_{l0}(r, \phi) = S_{l0}(r, \phi), \quad (10a)$$

$$B'_{l0}(r, \phi) = K_{l0}(r, \phi); \quad (\text{not used}) \quad (10b)$$

Spin-weight 1:

$$-A'_{l1}(r, \phi) = \frac{\partial S_{l1}(r, \phi)}{\partial r} + \frac{1}{r} \frac{\partial K_{l1}(r, \phi)}{\partial \phi}, \quad (11a)$$

$$-B'_{l1}(r, \phi) = \frac{1}{r} \frac{\partial S_{l1}(r, \phi)}{\partial \phi} - \frac{\partial K_{l1}(r, \phi)}{\partial r}; \quad (11b)$$

etc. The equations for spin-weight 2 and greater are straightforward to write down but are unwieldy and will not be used directly in that form anyway. It should be noted that the spin-weight 1 equations are a particular form of a Helmholtz decomposition.

The reason for starting with scalar fields S and K is that, being spin-weight 0, each can be expanded independently as a function of focal plane coordinates using ordinary Zernike polynomials. It is simplest to work with the Zernike polynomials expressed using complex notation. Let $C_n^m(r, \phi) = R_n^m(r)e^{im\phi}$, where any normalization, such as the Noll convention, is omitted; the convention here for negative angular index is that $R_n^{-m} = R_n^m$. The radius is in units of r_{max} , the radius of the focal plane field of view. One has:

$$S_{ls} = \sum_n \sum_m a_{nm}^{ls} C_n^m(r, \phi), \quad (12a)$$

$$K_{ls} = \sum_n \sum_m b_{nm}^{ls} C_n^m(r, \phi), \quad (12b)$$

where the sums extend over $m = -n$ to n but restricted to $m + n$ even; a_{nm}^{ls} and b_{nm}^{ls} are complex coefficients with the constraint that the coefficients are Hermitian on index m – i.e., coefficients of index $-m$ are the complex conjugates of the coefficients of index $+m$.

Upon substitution of Eqs. (12a) and (12b) into Eq. (9), one ends up with terms of the form $\delta^s C_n^m(r, \phi)$. One can define corresponding spin-weighted Zernike polynomials ${}_s C_n^m$ as follows:

$${}_s C_n^m(r, \phi) = (-1)^s \delta^s C_n^m(r, \phi) = {}_s R_n^m(r) e^{im\phi}. \quad (13)$$

The functions ${}_s R_n^m(r)$ are spin-weighted Zernike radial polynomials. A listing of the functions ${}_s C_n^m$ up to $n = 5$ is given in Appendix A. Note that the radial polynomials are of order $n - s$ in radius, so it is sometimes convenient to label them with $j = n - s$.

Unlike spin-weighted spherical harmonics, the spin-weighted Zernike polynomials (other than for $s = 0$), at least in this form, are not orthogonal on index n . However, one can orthogonalize them as follows. By inspection, the spin-weighted radial polynomials can be combined to create regular Zernike radial polynomials; in particular, one can write:

$$R_{n-s}^{m+s}(r) = \sum_{k \leq n} {}_s c_{nk} {}_s R_k^m(r), \quad (14)$$

where the ${}_s c_{nk}$ are numerical coefficients and $k + n$ is constrained to be even. For example, for $s = 1$, this equation becomes $R_{n-1}^{m+1} = ({}_1 R_n^m - {}_1 R_{n-2}^m)/(2n)$. Thus, one can convert the equations for the aberration coefficients from a sum over ${}_s R_n^m(r)$ to a sum (with different coefficients) over R_{n-s}^{m+s} , as follows:

$$(-1)^s (A'_{ls} + iB'_{ls}) = \sum_n \sum_m (a'_{nm}{}^{ls} - i b'_{nm}{}^{ls}) R_{n-s}^{m+s}(r) e^{im\phi}, \quad (15)$$

where the coefficients $a'_{nm}{}^{ls}$ and $b'_{nm}{}^{ls}$ are again complex. $R_{n-s}^{m+s}(r) e^{im\phi}$ is an orthogonal form for the spin-weighted Zernikes. The constraints are now $-n \leq m \leq n - 2s$, $n - s \geq 0$, $n + m$ even, and the coefficients are again Hermitian on index m . This last constraint follows as a consequence of the fact that the coefficients in Eq. (14) are independent of m . This formulation has the additional advantage that it is easier to implement than the original (nonorthogonal) equations. The one drawback (should it matter) of the orthogonal form is that the connection of the $a'_{nm}{}^{ls}$ and $b'_{nm}{}^{ls}$ to the original coefficients in the scalar equations (12a) and (12b) is somewhat complicated. Details are presented in Appendix B.

For computational purposes, the sums over complex functions can be rewritten as sums over real functions. Splitting the complex coefficients into real and imaginary components (where c and s are used to label cosine and sine coefficients respectively):

$$a'_{nm}{}^{ls} = a'_{nm,c}{}^{ls} - i a'_{nm,s}{}^{ls}, \quad (16a)$$

$$b'_{nm}{}^{ls} = b'_{nm,c}{}^{ls} - i b'_{nm,s}{}^{ls}, \quad (16b)$$

one has:

$$\begin{aligned} (-1)^s A'_{ls} &= \sum_n \sum_m [a'_{nm,c}{}^{ls} \cos m\phi + a'_{nm,s}{}^{ls} \sin m\phi] [R_{n-s}^{-m+s}(r) + R_{n-s}^{m+s}(r)] [1 - \delta_{m0}/2] \\ &\quad + \sum_n \sum_m [-b'_{nm,c}{}^{ls} \sin m\phi + b'_{nm,s}{}^{ls} \cos m\phi] [R_{n-s}^{-m+s}(r) - R_{n-s}^{m+s}(r)], \end{aligned} \quad (17a)$$

$$\begin{aligned} (-1)^s B'_{ls} &= \sum_n \sum_m [-a'_{nm,c}{}^{ls} \sin m\phi + a'_{nm,s}{}^{ls} \cos m\phi] [R_{n-s}^{-m+s}(r) - R_{n-s}^{m+s}(r)] \\ &\quad - \sum_n \sum_m [b'_{nm,c}{}^{ls} \cos m\phi + b'_{nm,s}{}^{ls} \sin m\phi] [R_{n-s}^{-m+s}(r) + R_{n-s}^{m+s}(r)] [1 - \delta_{m0}/2]. \end{aligned} \quad (17b)$$

These equations are the desired result. δ_{m0} is the Kronecker delta. The sums are now over $m = 0$ to n , again restricted to $m + n$ even, $m \leq n$, and $n - s \geq 0$. The individual terms

on the right side are the even and (negative) odd components of the spin-weighted radial polynomials with respect to m . For $n - s < m + s$, the term $R_{n-s}^{m+s}(r)$ in Eqs. (17a) and (17b) is 0, and the equations become two-fold degenerate between the a and b coefficients; for these terms, the b coefficients (corresponding to the B mode) are set to 0.

To recap, these equations provide a mechanism to parametrize the aberration coefficients (A' , B') (expressed in a radially aligned pupil coordinate system) as a function of position in the focal plane. Each aberration type is specified by the values of (l, s) (e.g., coma corresponds to $l = 3, s = 1$ while astigmatism corresponds to $l = 2, s = 2$). The number of terms on the right side of the equations [each term specified by (n, m)] required to characterize a pattern across the focal plane depends on the details of the optical system. Each term is a polynomial in radius of degree $n - s$ and harmonic in azimuth angle of order m . For each (n, m) combination, there are 4 coefficients, two for the E mode (a) and two for the B mode (b). In practice, one might have a map (either from raytracing or from direct measurement) of the (A' , B') aberration coefficients for each aberration type as a function of position in the focal plane, and the coefficients on the right side of Eqs. (17a) and (17b) are determined either from a least-squares fit to that map or, if coverage is uniform, from taking the inner product of map with each term (since the terms are orthogonal).

Sometimes it is useful to know the average power for a particular (A' , B') combination over the focal plane. This quantity can be computed from Eqs. (17a) and (17b), along with the orthogonality relations for Zernike polynomials, yielding:

$$\begin{aligned} \langle A'^2_{ls} + B'^2_{ls} \rangle &= \sum_n \sum_m \left[(a'_{nm,c})^2 + (a'_{nm,s})^2 + (b'_{nm,c})^2 + (b'_{nm,s})^2 \right] \\ &\times [1 - \delta_{m0}/2]/[n - s + 1] \end{aligned} \quad (18)$$

Finally for completeness, the average power in wavefront errors at a particular place in the focal plane can be computed from Eq. (1):

$$\langle W^2 \rangle = \sum_l \sum_s \frac{1}{2} (A'^2_{ls} + B'^2_{ls}) (1 + \delta_{s0}) / (2l + 2) \quad (19)$$

It is worth noting that, for the case $s = 1$, [Zhao & Burge \(2007, 2008\)](#) derived essentially all the results presented here (albeit for a slightly different application involving distortion and optics testing) but for a coordinate system that is Cartesian-aligned. Indeed, it is possible to express the spin-weighted Zernikes in Eqs. (17a) and (17b) using their ‘‘S’’ and ‘‘T’’ polynomials combined with a rotation. Appendix C provides more detail.

The difference between E-mode and B-mode patterns for one particular (n, m) combination is shown graphically in Fig. 3. [These modes correspond to S_7 and T_8 of [Zhao & Burge \(2007, 2008\)](#), now drawn side-by-side and at higher resolution.] For the B-mode, two centers of vorticity are clearly seen at $X = \pm 234$. At the periphery of the field, the E-mode vectors are primarily radial, while the B-mode vectors are primarily tangential. The equations for each mode in this figure are given in Table 2.

Spin-weighted functions offer at least two benefits for parametrizing aberration coefficients compared to previous approaches. First, the pupil wavefront coefficients A'_{ls} and

Table 1. Equations for Patterns in Fig. 3

Mode	Term	A' (Radial)	B' (Tangential)
E	$a'_{31,s}{}^{l1}$	$(3r^2 - 1) \sin \phi$	$(r^2 - 1) \cos \phi$
B	$b'_{31,c}{}^{l1}$	$-(r^2 - 1) \sin \phi$	$-(3r^2 - 1) \cos \phi$

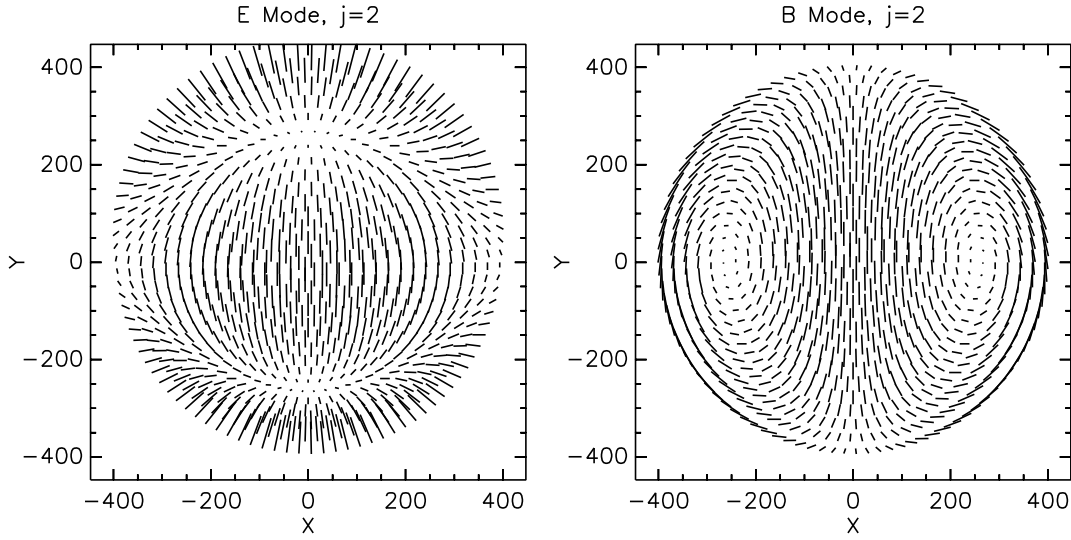


Figure 3. Aberration patterns for spin-weight 1 quantities (distortion, coma) for $n = 3$, ($j = 2$), $m = 1$. Left: E-mode. Right: B-mode. The axes are in units of mm (corresponding to the DESI focal plane described in section 3.) The lengths the tick marks are in arbitrary units.

B'_{ls} are referenced to radial and tangential directions respectively in the focal plane, and thus, for an axisymmetric system, all of the coefficients that characterize the spatial dependence are zero except for the $a'_{mn,c}{}^{ls}$ terms with $m = 0$. As is shown in Appendix C, even for nonaxisymmetric systems, the use of radial and tangential pupil coordinates results in equations that are more symmetrical than those using Cartesian pupil coordinates. (The precise choice for the center of the polar coordinate system is not important - picking a different center would result in a modification of all coefficients, but the form for all the equations would remain unchanged.) Second, the $b'_{nm}{}^{ls}$ coefficients, corresponding to the B mode (K) in Eq. (9), are usually negligible unless the misalignment patterns are induced by multiple, sufficiently strong, perturbations. Thus, spin-weighted functions offer an efficient way to represent aberration patterns.

3. APPLICATIONS

Two applications will be considered here – one involving the misalignment of a telescope, and the second being the mapping of distortion patterns.

3.1. Telescope Misalignment

The first example is quite simple – a Ritchey-Chrétien (RC) telescope in which the secondary mirror has been displaced and tilted. (Similar examples are commonly analyzed in the literature.) Telescope parameters are given in Table 2. (The unperturbed parameters correspond to an example used by [Schroeder 1987](#)). An RC design is optimized to have no third-order coma when properly aligned; the next highest aberration, astigmatism, is intrinsic to the design and has a pattern like that shown in Fig. 2, left side. This aberration corresponds to the term $j = 2, m = 0$.

The telescope is misaligned by offsetting the secondary mirror from the optical axis of the primary mirror by 5 mm and tilting the secondary to reobtain the best possible images. A conceptual repointing of the telescope is also done to recenter the field. Table 3 list the major residual perturbations induced by this misalignment, one term for coma and two terms for astigmatism. As is well known, a tilt and offset can be combined to eliminate coma at the field center. Here, the optimizer retains a small amount of coma of constant amplitude and orientation in order to balance astigmatism and produce the best images. These patterns are all E-mode.

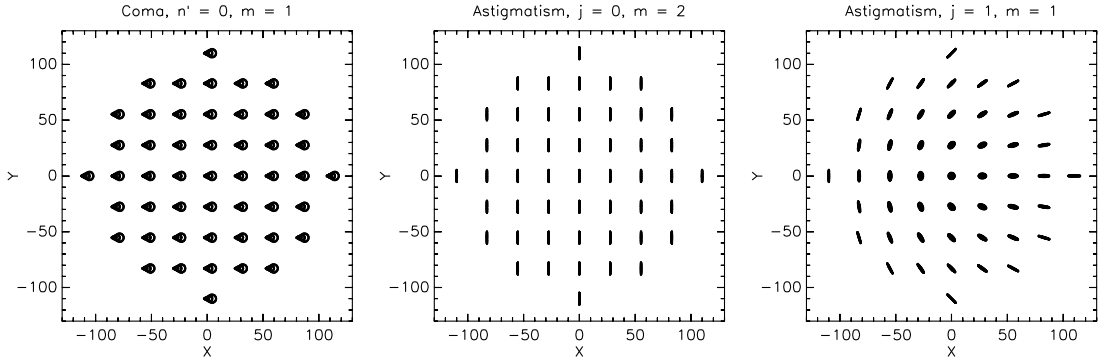
Figure 4 is a pictorial demonstration of the incremental patterns produced by each term. (Once again, for astigmatism, the focus is shifted slightly to highlight the orientation of the pattern.)

Table 2. Parameters of Ritchey Chretien Telescope

Surface	Parameter	Value	units
Primary	Diameter	4000	mm
	Radius of curvature	-20000	mm
	Conic constant	-1.0417	
	Distance to secondary	-7500	mm
Secondary	Radius of curvature	-6666.67	mm
	Conic constant	-3.1728	
	Offset	5	mm
	Tilt	0.119	deg
	Distance to Focus	10000	mm
Focal plane	Radius of curvature	-2655	mm
	Diameter	240	mm

Table 3. Aberration Coefficients for Perturbed RC Telescope

Mode	j	m	Amplitude	A' (Radial)	B' (Tangential)
Coma: $l = 3, s = 1$					
E	0	1	0.007	$\cos \phi$	$-\sin \phi$
Astigmatism: $l = 2, s = 2$					
E	0	2	-0.181	$\cos 2\phi$	$-\sin 2\phi$
E	1	1	0.962	$r \cos \phi$	$-r \sin \phi$

**Figure 4.** Focal plane aberration patterns for RC telescope with offset, tilted secondary. X and Y axis units are mm. The aberration patterns are not to scale and are for illustrative purposes only.

3.2. DESI Distortion

The Dark Energy Spectroscopic Instrument (DESI), currently under construction, will have 5000 fiber positioners and will be used for a survey measuring redshifts of 30 million galaxies (DESI Collaboration 2016a,b). It will be mounted at the prime focus of the Mayall telescope, at Kitt Peak in Arizona. A new, wide-field corrector will provide a 3 degree diameter field of view. In addition to the fiber positioners, the DESI focal plane will be equipped with a set of fixed fibers with good metrology that will act as fiducial points to calibrate the geometry of the focal plane. Both the positioner and fiducial fibers will be back-illuminated and imaged with a Fiber View Camera (FVC), which will be mounted near the primary mirror vertex. Because the FVC will view the focal plane through the corrector, it will be necessary to correct the positions measured by the FVC for distortion in the corrector. The DESI corrector will incorporate an atmospheric dispersion compensator (ADC), which will have two surfaces wedged relative to the optical axis and which will introduce nonradial distortions. Figure 5 shows the incremental distortion induced by the ADC with the lenses counter-rotated relative to the neutral position. It is seen that “vortic-

ity” is induced by the ADC. Thus, both E and B modes are needed to fully describe the pattern. The B mode, in fact, is the same as that shown in Fig.3.

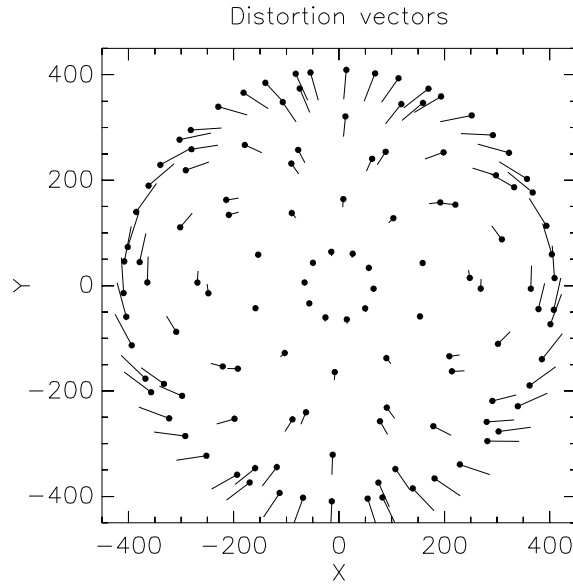


Figure 5. Incremental distortion in DESI corrector induced by counter-rotating the lenses relative to the neutral position. The X and Y axes are in units of mm. The distortion “whiskers” have been scaled up in length by a factor 10^4 .

A “linear” mapping of the sky (or object plane) to the focal (image) plane would be as follows:

$$r = \theta/f, \quad (20)$$

where r is polar radius in the focal plane, θ is the radial angle on the sky away from the field center, and f is the scale factor (arcsec mm^{-1} or equivalent). The azimuthal angle ϕ is the same in both object and image planes. In the presence of distortion, the convention used here is for f to be chosen such that Eq. (20) is exact at the center and at edge of the focal plane. (Any azimuthal dependence of the scale factor is assumed to be averaged over.) Thus, the radial distortion is zero at both the center and the edge of the focal plane and non-zero in between, reaching over 6 mm at the maximum.

The interpretation of the various terms, along with their amplitudes at the edge of the field (in units of mm), is shown in Table 4.

Distortion corresponds to the $l = 1, s = 1$ terms in Eq. (1), with a proportionality constant that is not of concern here. Specifically, at a point (r, ϕ) , distortion in the radial and tangential directions is given by $\Delta r \propto A'_{11}$ and $\Delta t = r\Delta\phi \propto B'_{11}$ respectively. (Note: for practical convenience, a local Cartesian system is defined around the nominal object center such that one axis is aligned with the radius vector; Δr and Δt are actually measured as Cartesian offsets in that system.) The convention here is that these increments are the differences between the actual location in the focal plane for the centroid of an object and the location predicted by the linear mapping as defined above.

Table 4. Interpretation of full DESI parameters

Mode	j	m	cos	sin	Description
E	0	1	0.002	0.000	Focal Plane decenter
	1	0	-5.790	–	Scale factor
	2	1	0.000	0.092	Optical axis decenter
	3	0	5.738	–	3rd order radial distortion
	4	1	0.000	0.004	Higher order decenter
	5	0	0.054	–	5th order radial distortion
B	0	1	–	–	Not used
	1	0	0.000	–	Focal plane rotation
	2	1	0.111	0.000	Vorticity
	3	0	0.000	–	Cubic spiral
	4	1	0.000	0.000	Higher order vorticity
	5	0	0.000	–	Fifth order spiral

Once again, it is convenient to replace the radial index n with $j = n - s$ and $s = 1$, since the radial polynomials are of this order. In practice, only the $m = 0$ and $m = 1$ azimuthal terms are important for the DESI distortion pattern, and the b terms for $j = 0$ are degenerate with the a terms and are set to 0. The pattern predicted by raytracing is fully described by terms up to $j = 5$, with an rms error of 1 micron. The B mode contributes about 111 microns (approximately one fiber diameter) at maximum rotation of the ADC. The total number of coefficients included is 16 (although several are essentially 0 and may be unnecessary once the actual corrector is assembled and tested.) For comparison, a more conventional Cartesian expansion requires 42 terms (e.g., [Anderson & King 2003](#), extended to 5th order). (For completeness, there are an additional two terms used to define the center of the sky or FVC pattern; these are computed by averaging the positions of all the fiducial spots in the FVC CCD, with no further adjustment.)

4. CONCLUSIONS

A method has been presented in which Zernike aberration coefficients are expressed in radially-oriented pupil coordinates so as to treat axisymmetric and non-axisymmetric optical systems on an equal footing. The method is general to arbitrary order in both azimuth and angular order in the focal plane and to arbitrary order of aberration.

The algorithms for distortion are currently incorporated in the DESI application “PlateMaker”, which is used for measuring distortion and mapping the focal plane to the sky. They have already been applied to data obtained with a prototype instrument “protoDESI” ([Fagrelius et al. 2016, 2017](#)) to analyze the behavior and stability of the instrument.

Aberration patterns other than distortion can be measured using wide-field exposures of defocused “donut” images of stars, as is currently done for the Dark Energy Camera (DECam; [Flaugher et al. 2015](#)) at CTIO ([Roodman et al. 2014](#)). Analysis of donut data from DECam using the methods presented here is currently in progress and will be reported elsewhere. These methods will also be of value in the future for analyzing images from wide-field telescopes such as LSST.

Finally, E/B mode decomposition may be of benefit for analyzing aberration patterns of off-axis telescopes, where, for certain designs, both E and B modes might be expected.

The author would like to thank Mike Lampton and Albert Stebbins for many stimulating discussions that contributed to the results presented here, and to Tod Lauer, Connie Rockosi, Paul Martini, Liz Buckley-Geer, and the referee for carefully reading the manuscript and providing invaluable feedback that greatly improved its clarity.

This manuscript has been authored by Fermi Research Alliance, LLC under Contract No. DE-AC02-07CH11359 with the U.S. Department of Energy, Office of Science, Office of High Energy Physics. The United States Government retains and the publisher, by accepting the article for publication, acknowledges that the United States Government retains a non-exclusive, paid-up, irrevocable, world-wide license to publish or reproduce the published form of this manuscript, or allow others to do so, for United States Government purposes.

APPENDIX

A. SPIN-WEIGHTED ZERNIKE POLYNOMIALS

Table 5 provides a list of the non-orthogonal form of spin-weighted Zernike polynomials ${}_s C_n^m$ up to $n = s = 5$.¹ Terms not listed are 0. Note that all terms with $n - s < m + s$ are 0.

Table 5. Spin-Weighted Zernike Polynomials

Spin-weight 0		
$C_0^0 = 1$	$C_1^{-1} = r e^{-i\phi}$	$C_1^1 = r e^{i\phi}$
$C_2^{-2} = r^2 e^{-2i\phi}$	$C_2^0 = 2r^2 - 1$	$C_2^2 = r^2 e^{2i\phi}$
$C_3^{-3} = r^3 e^{-3i\phi}$	$C_3^{-1} = (3r^3 - 2r) e^{-i\phi}$	$C_3^1 = (3r^3 - 2r) e^{i\phi}$
$C_3^3 = r^3 e^{3i\phi}$	$C_4^{-4} = r^4 e^{-4i\phi}$	$C_4^{-2} = (4r^4 - 3r^2) e^{-2i\phi}$
$C_4^0 = (6r^4 - 6r^2 + 1)$	$C_4^2 = (4r^4 - 3r^2) e^{2i\phi}$	$C_4^4 = r^4 e^{4i\phi}$
$C_5^{-5} = r^5 e^{-5i\phi}$	$C_5^{-3} = (5r^5 - 4r^3) e^{-3i\phi}$	$C_5^{-1} = (10r^5 - 12r^3 + 3r) e^{-i\phi}$
$C_5^1 = (10r^5 - 12r^3 + 3r) e^{i\phi}$	$C_5^3 = (5r^5 - 4r^3) e^{3i\phi}$	$C_5^5 = r^5 e^{5i\phi}$
Spin-weight 1		
${}_1 C_1^{-1} = 2e^{-i\phi}$	${}_1 C_2^{-2} = 4r e^{-2i\phi}$	${}_1 C_2^0 = 4r$
${}_1 C_3^{-3} = 6r^2 e^{-3i\phi}$	${}_1 C_3^{-1} = (12r^2 - 4) e^{-i\phi}$	${}_1 C_3^1 = 6r^2 e^{i\phi}$
${}_1 C_4^{-4} = 8r^3 e^{-4i\phi}$	${}_1 C_4^{-2} = (24r^3 - 12r) e^{-2i\phi}$	${}_1 C_4^0 = 24r^3 - 12r$
${}_1 C_4^2 = 8r^3 e^{2i\phi}$	${}_1 C_5^{-5} = 10r^4 e^{-5i\phi}$	${}_1 C_5^{-3} = (40r^4 - 24r^2) e^{-3i\phi}$
${}_1 C_5^{-1} = (60r^4 - 48r^2 + 6) e^{-i\phi}$	${}_1 C_5^1 = (40r^4 - 24r^2) e^{i\phi}$	${}_1 C_5^3 = 10r^4 e^{3i\phi}$
Spin-weight 2		
${}_2 C_2^{-2} = 8e^{-2i\phi}$	${}_2 C_3^{-3} = 24r e^{-3i\phi}$	${}_2 C_3^{-1} = 24r e^{-i\phi}$
${}_2 C_4^{-4} = 48r^2 e^{-4i\phi}$	${}_2 C_4^{-2} = (96r^2 - 24) e^{-2i\phi}$	${}_2 C_4^0 = 48r^2$
${}_2 C_5^{-5} = 80r^3 e^{-5i\phi}$	${}_2 C_5^{-3} = (240r^3 - 96r) e^{-3i\phi}$	${}_2 C_5^{-1} = (240r^3 - 96r) e^{-i\phi}$
${}_2 C_5^1 = 80r^3 e^{i\phi}$		
Spin-weight 3		
${}_3 C_3^{-3} = 48e^{-3i\phi}$	${}_3 C_4^{-4} = 192r e^{-4i\phi}$	${}_3 C_4^{-2} = 192r e^{-2i\phi}$
${}_3 C_5^{-5} = 480r^2 e^{-5i\phi}$	${}_3 C_5^{-3} = (960r^2 - 192) e^{-3i\phi}$	${}_3 C_5^{-1} = 480r^2 e^{-i\phi}$
Spin-weight 4		
${}_4 C_4^{-4} = 384e^{-4i\phi}$	${}_4 C_5^{-5} = 1920r e^{-5i\phi}$	${}_4 C_5^{-3} = 1920r e^{-3i\phi}$
Spin-weight 5		
${}_5 C_5^{-5} = 3840e^{-5i\phi}$		

¹ By using Mathematica, the referee was able to express these functions in closed form involving the use of Jacobi polynomials.

B. ORTHOGONALIZATION OF SPIN-WEIGHTED FUNCTIONS

This section give the details of the orthogonalization process. Specifically, the goal is to show that, if one applies the spin-raising operator to an equation of the form given by Eq. (15), the resulting equation can be rewritten to once again have the form of Eq. (15) but with the spin-weight s incremented by 1. By repeating this process incrementally after each application of the spin-raising operator (starting with spin-weight 0), one has effectively achieved the orthogonalization process given by Eq. (14).

As an initial matter, Equation (15) can be written in a slightly different form by shifting the angular indices m and n as follows:

$$(-1)^s (A'_{ls} + iB'_{ls}) = e^{-is\phi} \sum_{n'} \sum_{m'} (a'_{n'm'} - i b'_{n'm'}) R_{n'}^{m'}(r) e^{im'\phi}, \quad (\text{B1})$$

where $n' = n - s$ and $m' = m + s$. In this form, the double sums are now symmetric about m' (i.e. m' goes from $-n'$ to n' , $m' + n'$ even) and the sum over n' starts at 0. The leading exponential is the term that rotates spin-weight s quantities from a Cartesian frame to a radial/tangential frame. Thus, the double sum gives the quantity $A + iB$, and the exponential converts it to $A' + iB'$. One twist, however, is that the coefficients a' and b' are Hermitian on m , not m' .

To simplify notation, the right side of Eq. (B1) is rewritten as follows, retaining just the a' coefficients and one value of m' :

$$\sum_{n'} a'_{n'} R_{n'}^{m'}(r) e^{i(m'-s)\phi}. \quad (\text{B2})$$

Applying the spin-raising operator, Eq. (8a), gives the expression:

$$\sum_{n'} a'_{n'} \left[\frac{d}{dr} - \frac{m'}{r} \right] R_{n'}^{m'}(r) e^{i(m'-s)\phi}. \quad (\text{B3})$$

Notably, the radial part of this expression does not depend on the spin-weight s . The next step involves replacing the sum over the radial functions (which now are not orthogonal) with a sum using different coefficients over regular Zernike radial polynomials. From Lukosz (1963), Eq. (A II.4b) and Janssen (2014), Eq. (8), one has:

$$\left[\frac{d}{dr} - \frac{m'}{r} \right] R_{n'}^{m'}(r) = 2n' R_{n'-1}^{m'+1} + \left[\frac{d}{dr} - \frac{m'}{r} \right] R_{n'-2}^{m'}(r). \quad (\text{B4})$$

Let:

$${}_1R_{n'}^{m'} = \frac{dR_{n'}^{m'}}{dr} - \frac{m'}{r} R_{n'}^{m'}, \quad (\text{B5})$$

where the notation is consistent with that used in Eq. (13). By substituting Eq. (B5) into Eq. (B4), one gets:

$${}_1R_{n'}^{m'} = 2n' R_{n'-1}^{m'+1} + {}_1R_{n'-2}^{m'}. \quad (\text{B6})$$

One can rewrite this equation as:

$$R_{n'-1}^{m'+1} = ({}_1R_{n'}^{m'} - {}_1R_{n'-2}^{m'})/2n'. \quad (\text{B7})$$

The difference equation can be solved easily to yield:

$${}_1R_{n'}^{m'} = \sum_k (2k)R_{k-1}^{m'+1}, \quad (\text{B8})$$

where the sum extends over $1 \leq k \leq n'$ subject to the constraint that k has the same parity as n' . By combining Eqs. (B8) with (B5) and substituting into Eq. (B3), one now has a (double) sum over ordinary Zernike radial polynomials. The double sum can be simplified by introducing new coefficients a'' as follows:

$$a'_{n'} = \frac{a''_{n'}}{2n'} - \frac{a''_{n'+2}}{2(n'+2)} \quad (\text{B9a})$$

$$a''_{n'} = 2n' \sum_k a'_k, \quad (\text{B9b})$$

where the latter sum starts at $k = n'$ and extends to the upper limit of the expansion over $a_{n'}$ with the constraint that k has the same parity as n' . In one last step, the indices can be shifted yet again: $n'' = n' - 1$, $m'' = m' + 1$, and the spin-raised equivalent of Eq. (B2) finally has the form:

$$\sum_{n''} a''_{n''} R_{n''}^{m''}(r) e^{i[m''-(s+1)]\phi}. \quad (\text{B10})$$

To summarize, the effect of applying the spin-raising operator is to shuffle the coefficients (replacing a sum over a' with a sum over a'') and increase the spin-weight s by 1.

The same equations also hold for the b coefficients. Because the equations for these coefficients do not depend on m (or m'), the new coefficients a'' and b'' remain Hermitian on m .

C. COMPARISON TO OTHER WORK

Zhao & Burge (2007, 2008) derived expansions for a distortion field (i.e., spin-weight 1) that are essentially identical to those here, except that they used a coordinate system that is Cartesian-aligned. The purpose here is to show how the two are connected. This connection will be demonstrated explicitly for one term from the 2007 paper, Table 4: S_{16} . In the notation of that paper, this term is given by:

$$S_{16} = \frac{1}{2}[\hat{i}(\sqrt{2}Z_{11} + Z_{12}) + \hat{j}Z_{13}]. \quad (\text{C1})$$

The Noll form of the Zernike polynomials is given by:

$$Z_{11} = \sqrt{5}R_4^0(r), \quad (\text{C2a})$$

$$Z_{12} = \sqrt{10}R_4^2(r) \cos 2\phi, \quad (\text{C2b})$$

$$Z_{13} = \sqrt{10}R_4^2(r) \sin 2\phi, \quad (\text{C2c})$$

with

$$R_4^0(r) = 6r^4 - 6r^2 + 1, \quad (\text{C3a})$$

$$R_4^2(r) = 4r^4 - 3r^2. \quad (\text{C3b})$$

These equations represent the Cartesian x -axis and y -axis components of a vector. In the notation of the present paper, these components are called A and B . Thus, one has $S_{16} = \hat{i}A + \hat{j}B$, with:

$$A = \frac{\sqrt{10}}{2}[R_4^0(r) + R_4^2(r) \cos 2\phi], \quad (\text{C4a})$$

$$B = \frac{\sqrt{10}}{2}R_4^2(r) \sin 2\phi. \quad (\text{C4b})$$

The conversion to radial and tangential components A' and B' is given by:

$$A' = A \cos \phi + B \sin \phi, \quad (\text{C5a})$$

$$B' = -A \sin \phi + B \cos \phi. \quad (\text{C5b})$$

Substituting, one gets:

$$A' = \sqrt{10}[R_4^2(r) \sin 2\phi \cos \phi + R_4^0(r) \sin \phi - R_4^2(r) \sin \phi \cos 2\phi], \quad (\text{C6a})$$

$$B' = \sqrt{10}[-R_4^2(r) \sin 2\phi \sin \phi + R_4^0(r) \cos \phi - R_4^2(r) \cos \phi \cos 2\phi]. \quad (\text{C6b})$$

Making use of relations for the products of trigonometric functions, one finally gets:

$$A' = \sqrt{10}[R_4^0(r) + R_4^2(r)] \cos \phi, \quad (\text{C7a})$$

$$B' = -\sqrt{10}[R_4^0(r) - R_4^2(r)] \sin \phi. \quad (\text{C7b})$$

By comparison with Eqs. (17a) and (17b), one sees that S_{16} corresponds to the $a'_{nm,c}{}^{ls}$ term with $s = 1, n = 5, m = 1$. (Likewise, S_{17} corresponds to the $a'_{nm,s}{}^{ls}$ term, T_{16} corresponds to the $b'_{nm,c}{}^{ls}$ term, and T_{17} corresponds to the $b'_{nm,s}{}^{ls}$ term.) Note that the form of Eqs. (C7a) and (C7b) is more symmetrical than that of (C4a) and (C4b) in that it does not mix together terms of different harmonic order m .

REFERENCES

- Agurok, I. 1998, Proc. SPIE, 3430, 80
- Akiyama, M. et al. 2008, Proc. SPIE, 7018, 2
- Anderson, J., & King, I. R. 2003, PASP, 115, 113
- Bernstein, G. et al. 2017, PASP, 129, 4503
- Born, M., & Wolf, E. (2000), "Principles of Optics (7th Edition)" (Cambridge University Press: Cambridge)
- Braat, J. J. M., & Janssen, A. J. E. M. 2013, JOSA A, 30, 1213
- DESI Collaboration 2016, arXiv:1611.00036
- DESI Collaboration 2016, arXiv:1611.00037
- Fagrelus, P. et al, 2016, Proc. SPIE, 9908,7
- Fagrelus, P. et al, 2017, arXiv:1710.08875
- Flaugher, B. et al. 2015, AJ, 150,150
- Goldberg, J. N. et al. 1967, J. Math. Phys., 8,2155
- Gray, R. W., & Rolland, J. P. 2015, JOSA A, 32, 1836
- Hamana, T. et al. 2013, PASJ, 65, 104
- Janssen, A. J. E. M. 2014, J. Opt. Soc. Am., 31, 1084
- Jarvis, M., Schechter, P., & Jain, B. 2008, arXiv:0810.0027
- Jee, M. J., & Tyson, J. A. 2011, PASP, 123, 596
- Kamionkowski, M., Kuposov, A., & Stebbins, A. 1997, Phys. Rev. D, 55, 7368
- Kent, S. M. et al. 2016, Proc. SPIE, 9908, 8
- Kwee, I. W., & Braat, J. J. M. 1993, Pure Appl. Opt., 2, 21
- Lukosz, W. 1963, Opt. Acta, 10, 1
- Manuel, A. M. 2009, PhD thesis, U. Arizona
- McLeod, B. A. 1996, PASP, 2, 217
- Newman, E., & Penrose, R. 1966, J. Math. Phys., 7, 863
- Noll, R. J. 1976, JOSA, 66, 207
- Roodman, A., Reil, K., & Davis, C. 2014, Proc. SPIE, 9145, 16
- Schechter, P., & Levinson, R. 2011, PASP, 123, 812
- Schroeder, D. 1987, "Astronomical Optics" (Academic Press:San Diego)
- Shack, R. V., & Thompson, K. 1980, Proc. SPIE, 251, 146
- Stebbins, A. 1996, arXiv:9609149
- Torres del Castillo, G. F. 1992, Rev. Mex. Fis., 38, 19
- Trevino, J. P. et al. 2013, Physiol. Opt., 33, 394
- Zaldarriaga, M., & Seljak, U. 1997, Phys. Rev. D., 55, 1830
- Zhao, C., & Burge, J. H. 2007, Opt. Expr., 15, 18015
- Zhao, C., & Burge, J. H. 2008, Opt. Expr., 16, 6586